Visualization of In-Plane Dispersion of Hole Subbands by Photoelectron Spectroscopy

Sakura Nishino Takeda, Naoto Higashi, and Hiroshi Daimon

Graduate School of Materials Science, Nara Institute of Science and Technology, Takayama, Ikoma, Nara 630-0192, Japan

(Received 13 February 2004; published 24 January 2005)

The in-plane dispersion of the hole subband (HSB) in a Si quantum well is obtained for the first time by applying angle-resolved photoemission spectroscopy and surface science techniques. The entire shape of the HSB over a wide ranged wave vector, including admixing of heavy and light hole subbands around the crossing point and the camelback structure inducing negative effective mass, is visualized directly. Energy separations between the subbands are quantitatively explained.

DOI: 10.1103/PhysRevLett.94.037401 PACS numbers: 78.67.De, 73.21.Fg, 79.60.Jv

Subbands in a quantum well (QW) are quantized electronic states of carriers confined in the narrow potential having degrees of freedom of motion in the other perpendicular (in-plane) directions. Such carrier confinement is now routinely realized in various semiconductor devices such as metal-oxide-semiconductor field-effect transistors or light-emitting diodes. These confined carriers move nearly freely with dispersive energy in the in-plane directions, forming standing waves with discrete energies in the confined direction. The subband structure directly affects the performance of those devices, and thus quantitative analysis is needed. In the case where valence electrons in semiconductors are confined to a nanosized potential well, subbands are created from the three components of the bulk valence band (heavy hole, light hole, and split-off bands). Because admixing is expected among these components, the in-plane dispersions of the hole subband (HSB) can be different from the original valence band. Figures 1(a)–1(d) explain such subband formations schematically. Several calculations [1–3] have indicated basic characteristics of the in-plane dispersions, including negative effective masses and couplings of the valence components. However, experimentally, no direct method for dispersion determination has been available. Thus, the validity of the calculations was checked using effective masses of HSBs obtained by cyclotron resonance [4] or Shubnikov–de Haas oscillations [5]. Recently, magneto-tunneling spectroscopy [6] and photoluminescence spectroscopy [7] have been developed to measure in-plane dispersion of hole subbands in GaAs. These methods are, however, indirect and not quantitative because they need to assume potential or unoccupied band dispersion, and have not been applied to Si due to some experimental limitations.

Angle-resolved photoemission spectroscopy (ARPES) [8] is the only method that directly probes the band dispersion of occupied electronic states, and its ability has been proven by various recent works on determining the band structure of various materials. To apply the ARPES to subbands, however, we have to prepare a QW near the surface without an oxide layer or external electric field, which makes it difficult to observe the photoelectrons properly. In this study, such QWs have been realized as inversion layers by utilizing an atomic metal layer as a built-in electrode. Metal atoms adsorbed on a semiconductor surface often form ordered structures having electronic states in the semiconductor band gap. Depending on the species and the structure of the adsorbed metal, the surface states act as donor-type or acceptor-type electronic states [9]. Acceptor-type surface states have a high density of states below the Fermi energy. Electron occupation in these surface states causes a negatively charged surface and

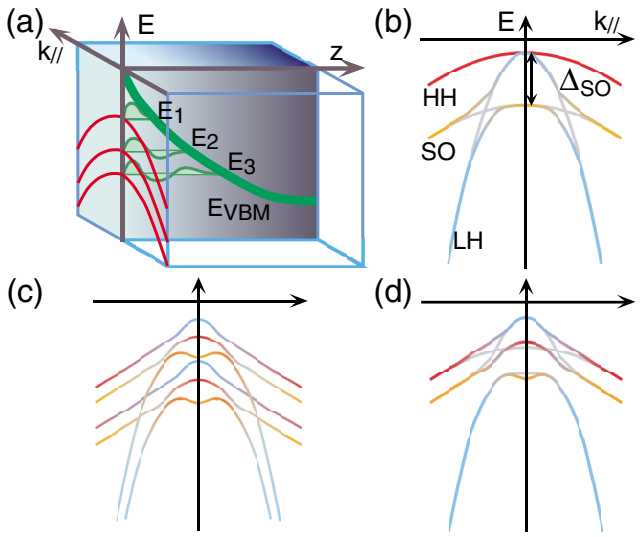

FIG. 1 (color). Schematic explanation of hole subbands in a p-channel inversion layer. (a) The electronic energy structure of a free electron confined in a p-type inversion layer, which shows multiple in-plane dispersions (E vs $k_{//}$). Line E_{VBM} is the maximum energy of the bulk valence band. (b) Practical valence band dispersion in bulk semiconductors showing heavy hole (HH: red line), light hole (LH: blue lines) and split-off band (SO: yellow lines). (c) Typical modification of those hole bands by their confinement in a narrow potential well. Degeneracy of HH and LH at gamma point is lifted. Colors of the lines express the couplings of the original bulk band components. (d) The three bands in (c) actually form quantized multiple subbands coupling with each other. Note that in-plane masses are employed to refer to each band.

induces upward band bending in the space-charge layer. Hole subbands are formed in this space-charge layer when the mean free path is longer than the confined width. The steepness of the space-charge layer is determined by the degree of the band bending and the width of the space-charge layer, which corresponds to the screening length for the penetrating electric field [denoted V and L in Fig. 2(a), respectively]. Because these values depend on the surface charge and carrier concentration in the substrate, the steepness of the space-charge layer is controllable.

We have studied the subband dispersions in several space-charge layers with different steepness by changing the substrate impurity concentration and/or the surface structure. Here we present the results of the HSB dispersion measurements in Si(111) p-type inversion layers. The samples are high-doped (impurity concentration of 1×10^{18} cm^3, named sample A) and low-doped (1.5×10^{15} cm^3, sample B) n-type Si(111) substrates. We employed a $\sqrt{7} \times \sqrt{3}$-In surface structure [10,11], which is one of the acceptor-type surface structures, as the built-in electrode. The $\sqrt{7} \times \sqrt{3}$-In surface structure consists of about one monolayer of indium with an atomic configuration close to the bulk indium crystal [11]. The electronic sturcture of $\sqrt{7} \times \sqrt{3}$-In consists of upward parabolic bands [12]. Electron occupation in these surface states induces strong upward band bending. In the photoemission spectra, the surface related bands disappear around the first Brillouin zone. This can be explained by the photoemission structure factor [13].

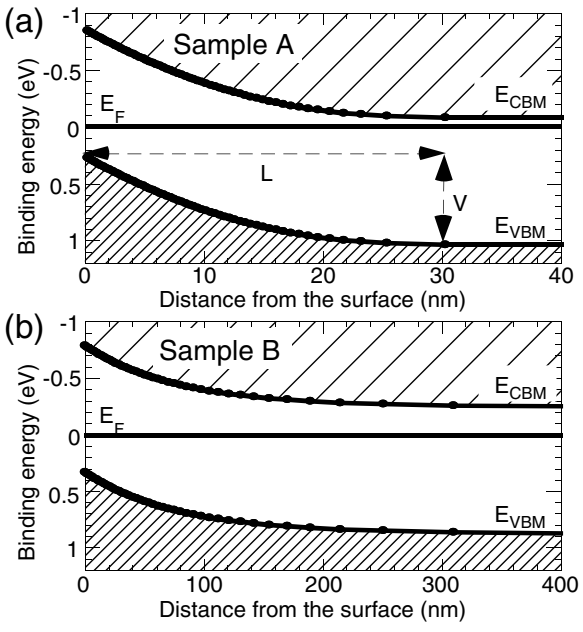

FIG. 2. Shape of the inversion layer calculated for (a) sample A (high-doped; Impurity concentration 1×10^{18} cm^{-3}) and (b) sample B (low-doped; 1×10^{15} cm^{-3}) Si(111) substrates covered with the $\sqrt{7} \times \sqrt{3}$-In structure. Lines E_{VBM} and E_{CBM} indicate energy levels for projected bulk valence band maximum and the conduction band minimum, respectively. V and L denote the amount of band bending and the width of the space-charge layer, respectively.

Surface preparations and photoemission measurements were done in an ultra-high-vacuum chamber to prevent surface contamination. Si(111) surface was heated by direct current to obtain a 7×7 reconstruction. After making $\sqrt{3} \times \sqrt{3}$-In [14] by depositing 0.3 monolayer In on heated sample, In was additionally deposited on the surface to make $\sqrt{7} \times \sqrt{3}$-In. The surface structure was carefully checked by reflection high-energy electron diffraction (RHEED). We confirmed no other surface structure than $\sqrt{7} \times \sqrt{3}$-In appeared in the RHEED pattern. The excitation light used for ARPES was monochromatic HeI (21.2 eV). Angular resolution of the photoemission spectrometer was 0.29°, which corresponds to momentum resolution of less than 0.01 Å^{-1} at E_F, and the energy resolution was 6 meV. The incident polar angle and azimuthal direction were 45° and $[\bar{1}10]$, respectively. The shape of the space-charge layer can be calculated using the Poisson equation under given boundary conditions, which are the energy positions of the valence band maximum (E_{VBM}) in the bulk and at the surface [15]. The E_{VBM} at the surface for each sample was monitored by surface core level shift obtained by photoemission spectroscopy. The measured E_{VBM} at the surface and the calculated shapes of the space-charge layers in both samples are shown in Fig. 2. The width L of the space-charge layer and surface carrier concentration are 30 nm and 4.5×10^{12} cm^{-2} for sample A and 300 nm and 1.0×10^{11} cm^{-2} for sample B.

ARPES revealed the multiple subbands in sample A. Figure 3(a) shows the photoelectron intensity map along the $[11\bar{2}]$ direction obtained from sample A. The bright area shows the dispersion of the occupied electronic state. The strong line B appearing in the binding energy region between 1.5 and 4.5 eV is a part of the Si bulk valence band [16], while the multiple subbands are seen at the binding energy range of 0.4–0.9 eV. There are two sets of bands with different curvature, and both sets consist of two or more bands. Here each component is denoted as HH_n and LH_n (suffix n is the number of the discrete levels from the top) in the figure analogous to the HH and LH in Fig. 1. This multiplet subbands structure suggests that the electrons are confined in a quantum well. Si inversion layer is the most responsible quantum well for the confinement in our system. Although In metal film can also act as a quantum well, existence of thick In metal film which causes multiplet states with energy separations of more than 100 meV is denied by both the amount of deposited In and RHEED patterns with low incident angles. Such clear subband features did not appear in the photoelectron intensity map from sample B. To compare the results from both samples, photoelectron spectra from samples A and B are shown in Figs. 3(b) and 3(c), respectively. The peaks denoted HH_n and LH_n in Fig. 3(b) correspond to those in

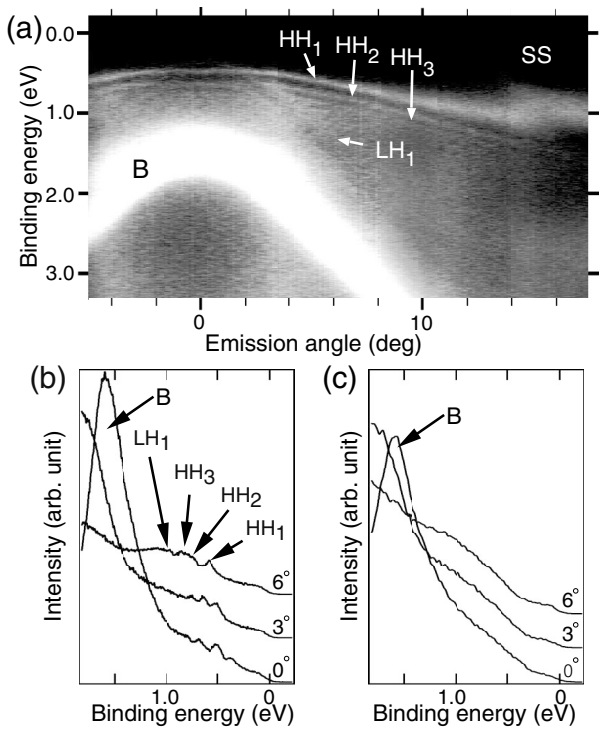

FIG. 3. Angle-resolved photoemission spectra for samples A and B. (a) An intensity plot of the photoemission spectra for sample A. The emission angle was changed along $[11\bar{2}]$. B and SS indicate Si bulk valence band and $\sqrt{7} \times \sqrt{3}$-In surface states, respectively. The spectra of the same data at the emission angles 0°, 3°, and 6° are shown in (b). (c) The corresponding spectra from sample B.

Fig. 3(a). There are no such clear peaks in Fig. 3(c), although a broad structure at around 0.7 eV is seen on each spectrum, which might be an indication of the existence of the peaks. To understand these multiplets, we roughly estimated the energy separation of discrete quantum levels for both samples using triangular approximation, which approximates the potential curves of Figs. 2(a) and 2(b) as triangles [17]. The discrete energy levels in a triangular potential well can be calculated exactly as

$$E_n = \left(\frac{\hbar^2}{2m_z^*}\right)^{1/3}\left(\frac{3\pi eF}{2}\left(n+\frac{3}{4}\right)\right)^{2/3},$$

where m_z^* is an electron effective mass along the direction perpendicular to the surface, and eF is the slope of the approximated linear potential. The calculated energy separations are $E_2 - E_1 = 134$ meV and $E_3 - E_2 = 110$ meV for sample A, and $E_2 - E_1 = 28$ meV, $E_3 - E_2 = 23$ meV for sample B. The measured energy separations for A are $E_2 - E_1 = 150$ meV and $E_3 - E_2 = 130$ meV, which are in qualitative agreement with the result from the calculation. On the other hand, the calculated energy separations for sample B are too small to be observed as individual peaks in the photoelectron spectra at room temperature. The broad structure appearing in the spectra for sample B may correspond to the set of peaks with small energy separations. The reported surface states [12] were observed in both samples. A part of them appears in the figure and is denoted as SS. Samples A and B are covered by the same surface structure and the difference between them is only the impurity concentration in the Si(111) substrate and the resulting space-charge layer width. This confirms that the observed bands HH and LH are the hole subbands. As far as we know, this is the first observation of the Si hole subband dispersion. Such hole subbands were not observed in Ref. [12] because the substrate used was p-type Si and the resulting band bending was downward. The surface states can penetrate into the bulk for several angstroms and one may consider an interaction between the surface states and the subbands in the inversion layer. At around gamma point, however, the region where the surface states occupy in (E, k) diagram is not coincident with that of the subband. Thus the band mixture between them cannot occur. At around larger k, where metallic surface states SS in Fig. 3(a) is close to the subbands in (E, k) space, subband peaks in the photoemission spectra become broader. This may be a trace of the interaction between them. Furthermore, a periodic potential of the surface structure might affect on the subband dispersion. This effect should be investigated in the further study.

Figures 4(a) and 4(b) are the detailed photoelectron spectra and their second derivative intensity map from sample A in the small energy and momentum ($k_{//}$) window around $k_{//} = 0$. Here, the horizontal axis of the intensity map is converted from angle θ to in-plane momentum $k_{//}$ using the relation

$$k_{//} = \frac{\sqrt{2m}}{\hbar}\sqrt{h\nu - \Phi - E_B}\sin\theta,$$

where Φ is the work-function of the sample. Besides the Si bulk valence band B at 1.5 eV, several subbands denoted as HH_n and LH_n are seen in Fig. 4(a). At small $k_{//}$ values, the subbands are close to each other and crossings or repulsions occur at $k_{//}$ around 0.05 $Å^{-1}$ (corresponding to 2° in the emission angle). Because the continuities of the bands at crossing/repulsion points are not clear on the map, we treated the bands in the smaller momentum region independently by giving them different notations (Γ_1–Γ_4) in Fig. 4(a) and 4(b). In the large momentum region, heavy hole bands HH_1, HH_{2-1}, HH_{2-2}, HH_3 and light hole bands LH_1 and LH_2 have dispersions similar to the respective valence band in the bulk. On the other hand, the bands around $k_{//} = 0$ (Γ_1–Γ_4) show dispersions that are different from the bulk band. Γ_2 and Γ_3, in particular, have upward curvature around $k_{//} = 0$. To see the dispersion of Γ_2 in more detail, the photoemission spectra of Γ_2 are shown in Fig. 4(c). With increases in the emission angle from 0°, the Γ_2 peak shifts to lower binding energy by 12 meV up to

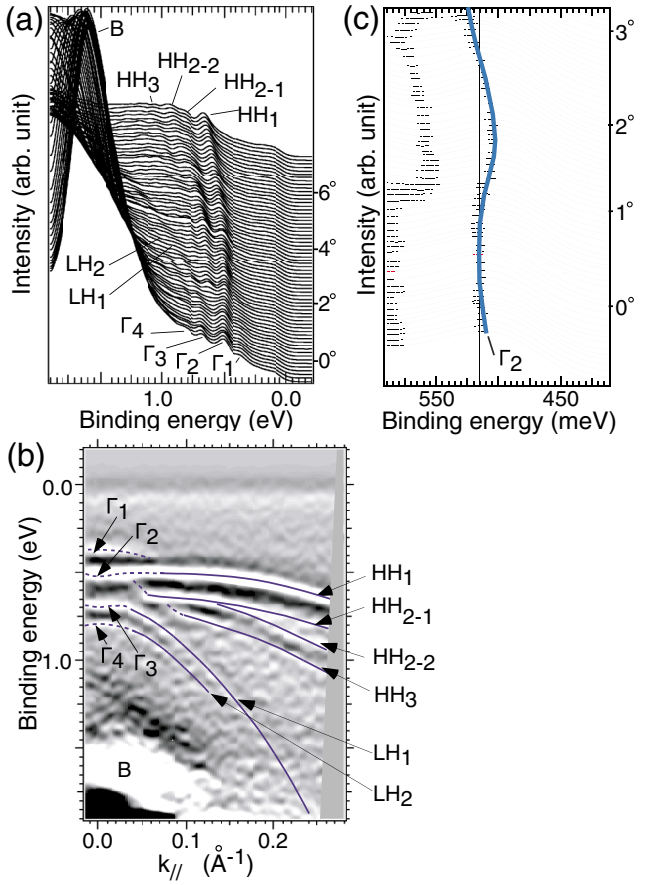

FIG. 4 (color). The detailed in-plane dispersion for sample A around $k_{//} = 0$. (a) Photoelectron spectra with the emission angle from $-1.19°$ to $7.11°$ (from bottom to top) in the $[11\bar{2}]$ direction. The emission angles are denoted at the right side of the graph. (b) A second derivative intensity plot in the conventional band diagram form obtained after converting the photoemission angle θ into momentum $k_{//}$. Dashed and solid lines are guides for the eye and represent the bands Γ_n and HH_n or LH_n, respectively. (c) The magnified spectra around Γ_2.

1.2° (corresponding to 0.04 $Å^{-1}$ in $k_{//}$), and then shifts to higher binding energy. This is the so-called ''camelback'' structure, which has negative effective mass. This structure indicates strong mixing between original light and heavy hole bands. The obtained depression energy is similar to the calculated values for Si(001) QW [2,3]. In Fig. 4(b), general features of HSB dispersion explained in Fig. 1 are seen. The degeneracy of LH and HH at $k = 0$ like Fig. 1(b) does not exist. The lifted degeneracy results in band repulsions (or crossings) in a same manner as Fig. 1(c). Furthermore, a mutliplet subband is formed due to discrete energy levels in confined direction and the the band diagram becomes more complicated as shown in Fig. 1(d). Lighter in-plane mass of Γ_1 at around $k_{//} = 0$ corresponds to the theoretical result that the ground subband has heavy mass character in the confined direction [2,3]. Recently photoemission spectroscopy was applied to two-dimensional electron gas formed in InAs accumulation layers by some groups [18,19]. Those groups succeeded in lowering the conduction band minimum below the Fermi level by alkali metal adsorption and detected the steplike density of states or parabolic dispersions at the bottom of the conduction subbands. In the case of present two-dimensional hole gas, ARPES detected the whole HSB structure because it exists under the Fermi level.

ARPES directly visualized the in-plane dispersion of HSB in the Si QW, including the complicated coupling of HSB and the negative effective mass, which have been predicted theoretically. A more detailed analysis of this system requires theoretical calculations. Since this method is applicable to other semiconductors, we believe that ARPES will become an indispensable tool to investigate the electronic structure in semiconductor QWs, which is important for fundamental physics and technological applications such as spintronics.

We gratefully acknowledge T. Ando for discussions. We thank N. Konno and H. Katagiri for their experimental assistance. This work was supported by a Grant-in-Aid for Specially Promoted Research Projects from the Ministry of Education, Science, Sports, and Culture, Japan.

[1] T. Ando, A. B. Fowler, and F. Stern, Rev. Mod. Phys. **54**, 437 (1982).
[2] S. Rodríguez, J. A.López-Villanueva, I. Melchor, and J. Carceller, J. Appl. Phys. **86**, 438 (1999).
[3] Y. T. Hou and M. F. Li, Jpn. J. Appl. Phys. **40**, L144 (2001).
[4] K. von Klitzing, G. Landwehr, and G. Dorda, Solid State Commun. **15**, 489 (1974).
[5] J. P. Kotthaus and R. Ranvaud, Phys. Rev. B **15**, 5758 (1977).
[6] R. K. Hayden *et al.*, Phys. Rev. Lett. **66**, 1749 (1991).
[7] J. A. Kash, M. Zachau, M. A. Tischler, and U. Ekenberg, Phys. Rev. Lett. **69**, 2260 (1992).
[8] S. Hüfner, *Photoelectron Spectroscopy* (Springer, Berlin, 1996).
[9] H. Lüth, *Surfaces and Interfaces of Solid Materials* (Springer-Verlag, Berlin, 1998), 3rd ed.
[10] S. Takeda, X. Tong, S. Ino, and S. Hasegawa, Surf. Sci. **415**, 264 (1998).
[11] J. Kraft, S. L. Surnev and F. P. Netzer, Surf. Sci. **340**, 36 (1995).
[12] E. Rotenberg *et al.*, Phys. Rev. Lett. **91**, 246404 (2003).
[13] H. Daimon, S. Imada, H. Nishimoto, and S. Suga, J. Electron Spectrosc. Relat. Phenom. **76**, 487 (1995).
[14] J. M. Nicholls, P. Mårtensson, G. V. Hansson, and J. E. Northrup, Phys. Rev. B **32**, 1333 (1985).
[15] W. Mönch, *Semiconductor Surfaces and Interfaces* (Springer, Berlin, 1995).
[16] R. I. G. Uhrberg *et al.*, Phys. Rev. B **31**, 3795 (1985).
[17] F. Stern, Phys. Rev. B **5**, 4891 (1972).
[18] M. G. Betti *et al.*, Solid State Commun. **110** 661 (1999).
[19] V. Yu. Aristov *et al.*, Phys. Rev. B **60**, 7752 (1999).